AIMS Materials Science, 13(1): 63–79.
DOI: 10.3934/matersci.2026004
Received: 15 October 2025
Revised: 14 December 2025
Accepted: 18 December 2025
Published: 12 January 2026

https://www.aimspress.com/journal/Materials

Research article

Effect of alumina nanoparticles on the microstructure, mechanical, and thermal properties of penta bismuth-tin-based solder alloys

Abbas Al-Bawee[1], Feryal Dawood[2] and Ahmed Alrubaiy[1,*]

[1] University of Diyala, College of Engineering, Baquba, Diyala, Iraq
[2] University of Diyala, College of Basic Education, Baquba, Diyala, Iraq

* **Correspondence:** Email: Ahmed_ail_eng@uodiyala.edu.iq.

Abstract: This study systematically investigated the thermal, mechanical, and structural properties of a bismuth-based (Bi-Pb-Sn-Cr-In) pentacrystalline structure solder matrix doped with nano-alumina powders to evaluate its characteristics at various nano-alumina loadings (0.5–1.5 wt%). Four well-designed nano-Al_2O_3 production alloys, differing only in nano-Al_2O_3 content, were synthesized and then investigated through X-ray diffraction, thermal/electrical transport tests, and elastic-hardness mapping methods to evaluate the effectiveness of the reinforcement. The results indicate that the presence of Al_2O_3 optimized the crystalline lattice of the alloy and effectively enhanced its mechanical properties, especially nano-Al_2O_3 at 1 wt%, which acted as a structural refiner, leading to the finest crystal domains and to the maximum Vickers microhardness value of 19.05 kg/mm^2. Thermal management of Al_2O_3 agglomerate improves thermal stability and mechanical strength by increasing the alloy's melting temperature and pasty range. The specified 1 wt% nano-Al_2O_3 reinforcement loading provides enhanced mechanical robustness, thermal endurance, and electrical conductivity, with outcomes such as extended operational lifespans, lower failure rates, and long-term reliability in electronic packaging systems.

Keywords: mechanical-thermal-electrical synergy; nano-alumina reinforced Bi-Sn solder; thermal properties; lead-free penta-alloy system; conductivity; melting point

1. Introduction

While Bi-Sn-based alloys offer low melting points, their application is often limited by intrinsic brittleness, low creep resistance, and coarsening microstructures during thermal cycling [1]. Incorporating ceramic nanoparticles like Al_2O_3 is a strategy established for microstructural refinement and dispersion strengthening in metallic matrices. This study, therefore, investigates the effect of nano-Al_2O_3 on the microstructure, hardness, and thermal stability of a complex Bi-Pb-Sn-Cr-In alloy, to investigate if optimal dispersion will refine grains, pin dislocations, and enhance thermal conductivity, thereby mitigating brittleness and improving overall reliability, rather than specifically targeting shear modulus enhancement. Al Katawy et al. [2] reported grain refinement in Bi-Ga austempered steels, illustrating the universality of dispersion-strengthening mechanisms. To reduce the susceptibility of bi-rich solders to thermal fatigue, micro-alloying with elements such as Se, In, Zn, and Al is recommended [3]. This process reduces the likelihood of thermal fatigue in the grains by refining them and enhancing their plasticity range. To achieve the appropriate melting point, mechanical strength, and reliability in Bi-Sn-based alloys, it is necessary to incorporate nano-alumina particles, typically ranging from 0.1 to 1.0 wt% [4]. This study seeks to attain the equilibrium in advanced electronic soldering by integrating nano-alumina into Bi-Sn alloys (Bi-Pb-Sn-Cr-In).

The microstructure of nano-alumina is precisely defined, facilitating the development of fine, uniformly distributed grains in the Bi-Sn solder, where Al_2O_3 nanoparticles function as effective boundary pinning agents and sites for heterogeneous nucleation. In a related investigation utilizing Bi-Ga austempering, Al Katawy et al. [2] achieved a 35% diminution in grain size. This illustrates the extensive potential of combined solute-drag effects and heterogeneous nucleation to enhance metallic microstructures.

Singh et al. [3] reported that the incorporation of nano-Al_2O_3 into Bi-Sn matrices enhances their strength by inhibiting dislocation mobility and grain-boundary sliding. This results in a 33% enhancement in microhardness and a 50% augmentation in shear strength. Yang's research [5] on aluminum addition to Sn-20Bi solder demonstrated significant hardness improvements, reaching a maximum of 27.1 HV at 0.5 wt% Al content, plateauing at 0.3 wt%. Amares et al. [6] found that adding 3% nano-Al_2O_3 to Sn-58Bi solder increased hardness to 17.1 HV on the Vickers scale.

Mechanical strengthening in these systems occurs primarily through microstructural refinement, as finer grain structures impede atomic dislocation motion. However, over-addition of aluminum triggers the formation of Al-rich particles that accelerate solid-state nucleation, reduce undercooling, and ultimately degrade the alloy's mechanical performance [7]. Literature consistently concludes that Al-bearing solders exhibit augmented shear resistance. Yang's work [8] on Sn-58Bi alloys demonstrates these modifications through superior shear values linked to Al-nanoparticle dispersions that stabilize the β-Sn microstructure even after prolonged exposure to 75 °C. Kang's investigation into Bi-Sn solders indicates that nanoparticle reinforcements, such as Ni-carbon nanotubes at concentrations of 0.05%–0.1%, enhance mechanical properties, particularly tensile strength, by facilitating load transfer through carbon nanotubes (CNTs) bridging. Additionally, Cu and Ni nanoparticles at 4% increase the hardness of Sn-58Bi solder by 16% and 23%, respectively [9]. Following 288 h of extended ageing at 85 °C, Al_2O_3 nanoparticles prevent intermetallic compounds from becoming excessively thick, restricting their thickness to 1.27 μm, thereby enhancing the stability of Sn-58Bi joints at the interface [10]. This enhances mechanical properties and demonstrates that nanoparticles could be used to enhance these properties, particularly during thermal cycling and electrical stress.

Compared to the base Sn-58Bi alloy, 3 wt% nano-Al_2O_3 lowers the melting point to 143.44 °C, which indicates that ceramic reinforcement plays an important role in thermal performance and extended compatibility with thermally sensitive electronic components. Bismuth is also very effective at lowering the melting point of solder alloys. When added to Sn-Ag-Cu (SAC) alloys, differential scanning calorimetry (DSC) analysis confirms this effect [11]. Consequently, Bi-containing solders are especially useful for soldering in low-temperature applications. Other metals that are added to Bi-Sn-based solders, like antimony (Sb), also alter heat-conducting properties. Adding Sb can raise the melting point [12,13]; in fact, the quinary alloy Sn-3.0Ag-0.5Cu-25Sb melts at 332.91 °C with a 28.74 °C pasty range, whereas supplementing Sn-0.3Ag-0.7Cu with 20% Bi significantly narrows the solid–liquid interval [12]. Adding cerium (Ce) can change how a material reacts to heat by changing how its microstructure changes during thermal cycling [14]. Akbar's research on Bi-Sn-based solders highlighted its effectiveness in enhancing performance by degenerating Cu_6Sn_5 and Ag_3Sn intermetallic compounds, thereby lowering the melting temperature [11]. Bi also improves the wettability of SAC solders and enhances their creep and thermal fatigue resistance [13]. This method provides a flexible way to change the thermal properties of Bi-Sn-based solders to suit different electron requirements.

The resistance of solder alloys to wetting is a critical property that directly influences their ability to establish robust connections in electronic devices. Previous studies [4,5,15] have contributed to our understanding of the behaviour of Bi-Sn-based solders with nano-alumina at the interface and under wetting conditions. Amares et al. [6] discovered that the substrate was effectively wet as the Sn-58Bi solder with 3% Al_2O_3 had a low contact angle of approximately 20.4°. Yang et al. [5] assert that the wettability response and the essential concentration threshold are determined by the aluminum dosage, which remains nearly constant when the aluminum content is ≤0.1 wt%. Sayyadi et al. [15] found that adding bismuth to SAC257 solder made it spread more easily, going from 80.46% to 85.97%, meaning that it was more wettable. Authors referred that bismuth improved the solder because it weakened the forces inside and lowered the overall surface tension of the molten solder. It also changed the fracture dynamics from Intermetallic Compounds control in the base solder joint to solder control in the bismuth-containing joint. This made the connections more reliable. Adding bismuth and reinforcing with nano-alumina can improve the wettability and interfacial properties of lead-free solders for electronic use. Yang's study showed that adding 0.5 wt% Sb to Sn-Bi solder decreases the grains and increases elongation by 40% [16].

Several other nanoparticle reinforcements have been tested to improve the properties of solder, and nano-alumina has shown promise as a reinforcement for Bi-Sn-based solders. Many researchers [9,17–20] have looked into different types of nanoparticles that can be used to strengthen these solders, including metallic nanoparticles like copper, nickel, cobalt, iron, and aluminum, as well as ceramic nanoparticles like TiO_2, Si_3N_4, ZrO_2, and Y_2O_3. Researchers have found that these nanoparticles reduce the width of the microstructure and improve mechanical properties. Adding metallic nanoparticles like copper and nickel increases hardness and elastic modulus [9]. Adding ceramic nanoparticles like TiO_2 and ZrO_2 to SAC107 lead-free solder improved its properties. Graphene nanosheets (GNSs) have been added to Sn-20Bi solder to investigate its use in new applications [20]. Researchers found that CNTs improve creep properties, tensile strength, and the material microstructure [17].

Table 1 shows a comparative overview of reinforcement strategies for multi-component, lead-free bismuth-tin solder alloys. Adding these particles to Bi-Sn-based solders improves the microstructure

and mechanical properties and slows down the growth of intermetallic compounds in the eutectic phase. This makes them a good choice instead of regular soldiers. While the present study focuses on singular Al_2O_3 reinforcement, there is parallel evidence that ZnO–carbon fiber hybrids are capable of exceeding the established 1 wt% Al_2O_3 ceiling [21]. Prior studies have demonstrated that controlled nano-reinforcements such as oxides, graphene, and metallic nanoparticles can refine microstructure and elevate mechanical integrity. Still, there is a major gap in our understanding of lead-free Bi-Sn solder alloys; previous works have not focused on reinforcement types, optimal loadings, and the ways in which dispersion strengthens the material.

This investigation aims to bridge this gap by introducing nano-Al_2O_3 (0–1.5 wt%) into a penta-component Bi-Pb-Sn-Cr-In matrix. While Sn-Bi-In systems are well-studied for ultra-low-temperature soldering [22,23], the present alloy incorporates Pb and Cr to explore a distinct compositional space. Pb is included in a research context to study its influence on the pasty range and fluidity in a complex system, whereas Cr serves as a micro-alloying agent for grain boundary modification. The primary novelty lies in evaluating how nano-Al_2O_3 interacts with and reinforces this specific multi-elemental matrix.

Table 1. Overview of reinforcement types, alloy matrices, and weight fractions used in recent experimental studies.

Reference	Reinforcement material	Solder alloy composition	Nanoparticle weight percentage
Said et al., 2019 [18]	TiO_2: refines microstructure and decreases melting temperature	Sn-1.0Ag-0.7Cu solder alloy with TiO_2 addition	0.25, 0.5, 0.75, and 1.0 wt% TiO_2
Yang et al., 2020 [20]	GNSs: improve wettability, inhibit IMC growth, refine microstructure, and enhance mechanical properties	Sn-20Bi solder alloy with GNSs	GNSs added at 0, 0.02, 0.04, 0.06, 0.08, and 0.1 wt%
Kang et al., 2021 [9]	Nanoparticles like Y_2O_3, Ti, Ni, Cu, and SnO_2 refine the microstructure and improve mechanical properties	Sn-58%Bi-based alloy, modified with Ag, Cu, In, Sb, Ti, Co, and Zn nanoparticles	Nanoparticles added: 0.5%–4% Cu, 0.5%–4% Ni, 0.03%–0.1% Cu_6Sn_5, 0.03% CNTs, 0.5% Ni, and 0.5% Zn
Fathy et al., 2025 [19]	WO_3 nanoparticles: improved microstructure, wettability, shear strength, and elongation	Sn-Bi alloy with 10 and 20 wt% Bi, reinforced with WO_3 nanoparticles	0.25–1.00 wt%

2. Materials and methods

Base metals (bismuth, lead, tin, chromium, and indium) were sourced with purity values ≥ 99.9% to ensure compositional fidelity during melting. The base alloy composition was fixed at $Bi_{50}Pb_{15}Sn_{22}Cr_3In_{10}$ (wt%). Melting was performed under a continuous nitrogen flow of 2.5 L/min using a rosin-based mildly activated flux for minimum oxidation. For Scanning Electron Microscope (SEM) analysis, solidified samples were mounted and sequentially polished with SiC papers (grades 240 to 2000) and diamond suspensions (3 and 1 mm), and finally etched with a 5% HNO_3 + 3% HCl + 92% C_2H_5OH solution for 10 s to reveal microstructural features. Following the predetermined compositional ratios, the charge was melted and allowed to solidify on substrates exposed to atmospheric conditions. To prevent aluminum from oxidizing, the melt was covered with a stream of

nitrogen gas, complemented by flux incorporation to minimize residual oxides and to sustain alloy wettability. Phase identification was performed with a Shimadzu Dx-30 diffractometer (Japan) operated at 45 kV/35 mA, Cu-Kα source, nickel filtration, and a constant angular sweep of 5°/min over 0–100°. A TA Instruments Universal V4.5A unit produced SC thermograms over 0–300 °C, applying a uniform heating rate of 10 K/min. The JEOL JSM-6510LV (SEM) was used for microstructural characterization, providing 300 times greater imaging depth than conventional optical techniques; it was used at 20 kV and 10 mm working distance, coupled with differential scanning calorimetry for precise thermodynamic parameter extraction. This supports robust correlations between observed microstructure and thermal behavior and precise extraction of thermodynamic parameters such as enthalpy, entropy, and melting point data.

3. Results

3.1. X-ray diffraction (XRD)analysis and structure

XRD analysis indicates that Bi-Sn solders exhibit a critical loading pattern for nano-Al_2O_3. Similar to the TiO_2, WO_3, and GNS reinforcements presented in Table 1, this achieves an optimal equilibrium between strength and electrical and thermal conductivity. The bi-rich platelets and the predominant β-Sn phase exhibit distinctly sharp peaks, as illustrated in Figure 1. The Cr-In intermetallic, on the other hand, has only small peaks. Consistent with the grain-refinement trends reported by Dawood et al. [1] for Se-In-Zn-Al-modified Sn-43Bi solders, non-reinforced alloys exhibit coarse crystallites (~357 nm) that enable unrestricted grain growth. The increased size of the crystallites (around 357 nm) and the high lattice parameters (a = 4.748 Å and c = 11.87 Å) indicate that the grains are rough and there is minimal distortion, as shown in Table 2. Without reinforcement, grains can grow freely, which makes the microstructure brittle and lamellar. This is in line with the findings of previous studies [3,6] in non-reinforced Sn-Bi systems.

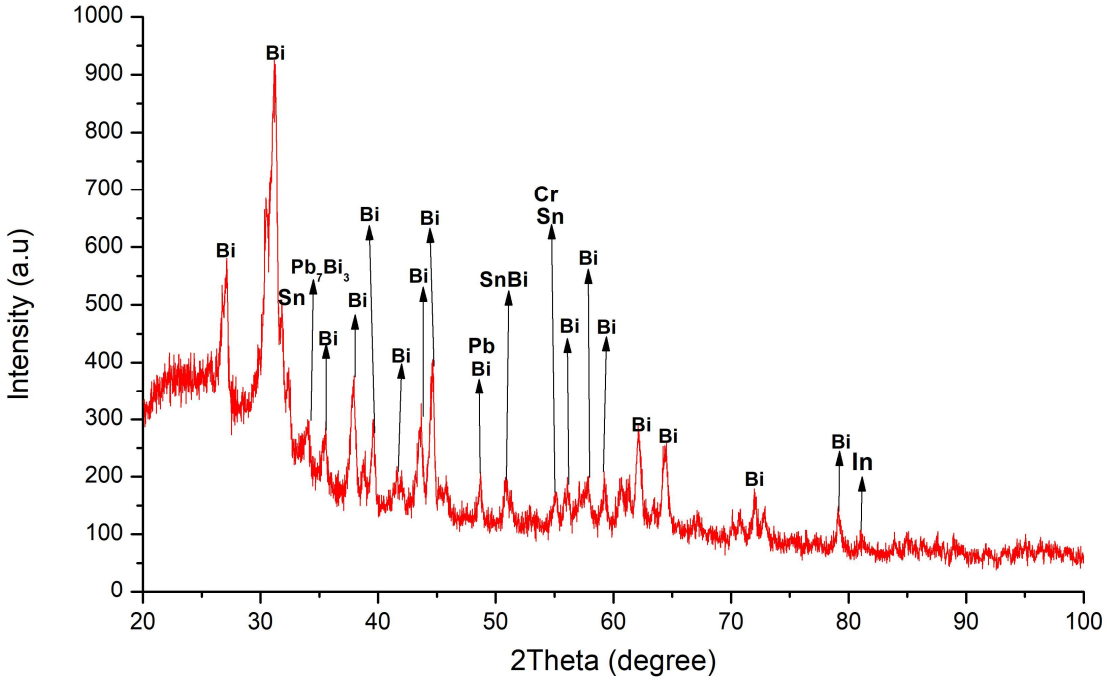

Figure 1. XRD pattern of $Bi_{50}Pb_{15}Sn_{22}Cr_3In_{10}$ alloy without alumina reinforcement.

Table 2. Effect of nano-Al_2O_3 on lattice constants, unit cell volume, and particle size of penta bismuth-tin solder alloys.

Composition	a_{rho} (Å)	c (Å)	Unit cell volume (Å^3)	Particle size (Å)
$Bi_{50}Pb_{15}Sn_{22}Cr_3In_{10}$	4.748	11.87	70.766	357.64
$Bi_{49.5}Pb_{15}Sn_{22}Cr_3In_{10}(Al_2O_3)_{0.5}$	4.676	11.61	69.296	283.29
$Bi_{49}Pb_{15}Sn_{22}Cr_3In_{10}(Al_2O_3)_1$	4.681	11.625	69.437	356.94
$Bi_{48.5}Pb_{15}Sn_{22}Cr_3In_{10}(Al_2O_3)_{1.5}$	4.789	12.01	71.774	301.45

Peak broadening, accompanied by a subtle high-angle displacement in Figure 2, indicates a crystallite size decrease to ~283 nm, whereas the appearance of Al_2O_3 peaks at 35 and 43° substantiates nanoparticle integration. Figure 2 also shows that 0.5 wt% nano-Al_2O_3 addition acts as a heterogeneous nucleation site and reduces Sn-Bi grain size. The result found in Yang et al. [5] is similar: adding 0.5 wt% Al_2O_3 decreased the grain size of the Sn-Bi by about 20%.

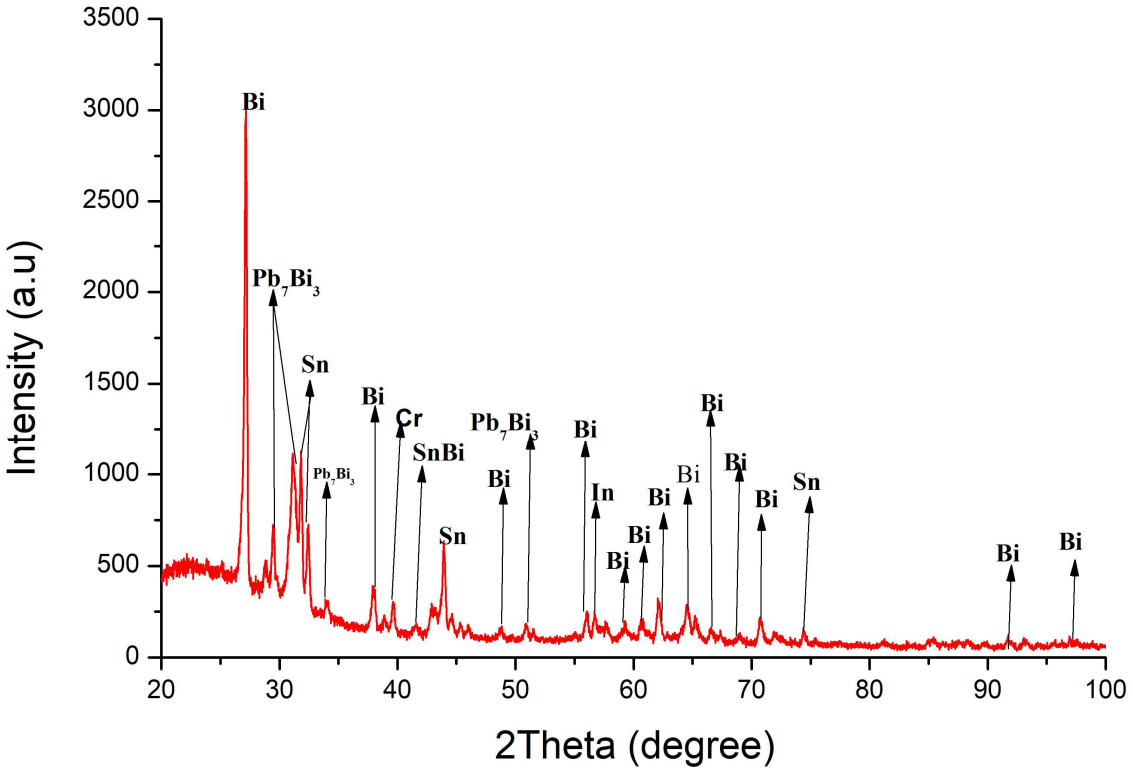

Figure 2. XRD profile showing initial refinement of crystalline phases due to 0.5 wt% Al_2O_3 addition.

Figure 3 demonstrates that 1 wt% Al_2O_3 loading simultaneously minimizes crystallite dimensions (about 301 nm), maximizes peak broadening, and maintains a homogeneous strain, resulting in an optimal dispersion equilibrium. This important threshold was reached, which backs up the results of Fathy et al. [19] on WO_3/Sn-Bi, who found that 1 wt% led to the best grains and hardness. Peak sharpening and intensity recovery in crystallite size with excess Al_2O_3 (~301 to 356 nm) are revealed in Figure 4. Nanoparticle clustering decreases nucleation sites and re-coarsens the microstructure, suggesting agglomeration-induced Ostwald ripening. Consistent with Li et al. [10], 15% grain coarsening

and IMC thickening are caused by excessive Al_2O_3 in Sn-58Bi. The best refinement happens at 1 wt%, while too much loading (>1 wt%) makes coarse microstructures stronger, showing how likely nanoparticles are to clump together. There is a nonlinear, inverted U relationship between the amount of Al_2O_3 and the refinement of the microstructure, peaking at 1 wt%. When the agglomeration threshold is 1.5 wt% or higher, nanoparticles start to group together, which cancels out the benefits of dispersion. As the lattice parameters get smaller, up to 1 wt%, dislocation pinning and hardness improve (Table 2).

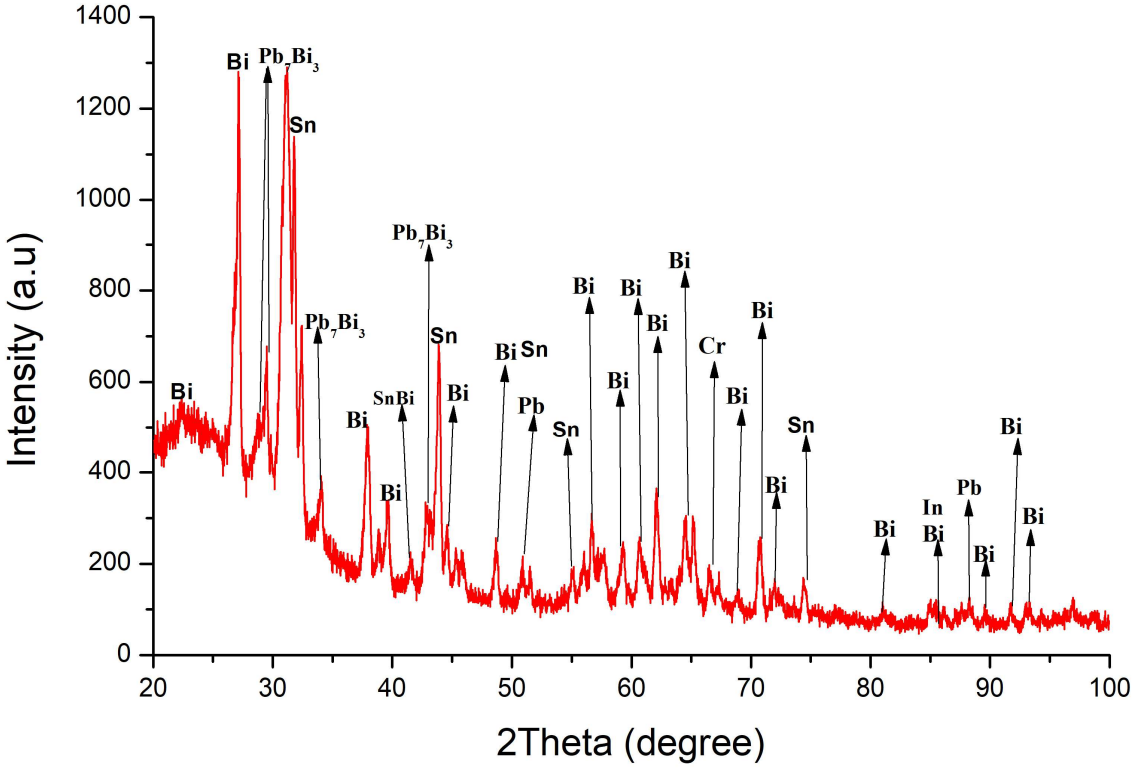

Figure 3. XRD analysis revealing optimum phase refinement at 1 wt% Al_2O_3 in a Bi-based alloy.

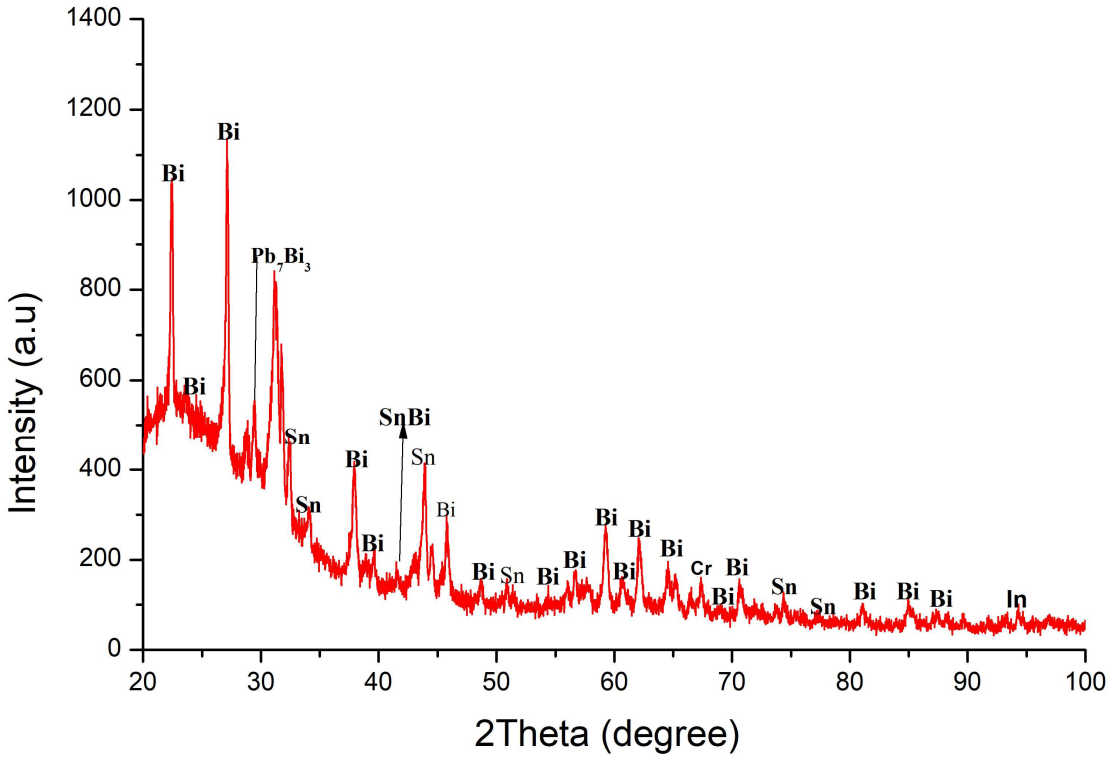

Figure 4. XRD spectrum of Bi-based alloy containing 1.5 wt% Al_2O_3 showing potential agglomeration effects.

3.2. SEM evaluation

The unreinforced $Bi_{50}Pb_{15}Sn_{22}Cr_3In_{10}$ (0 wt% Al_2O_3) has rough, dissimilar dendrites of β-Sn surrounded by Bi-rich lamellae. It also has significant shrinkage porosity and few Cr-In intermetallics, as seen in Figure 5. Without pinning agents, solid-state diffusion can easily occur, which means that large grains can crack more easily. This topography is similar to the micrographs by Yang et al. [5] for Sn-20Bi, where the dendritic coarseness was similar, and the hardness was low (9.7 HV).

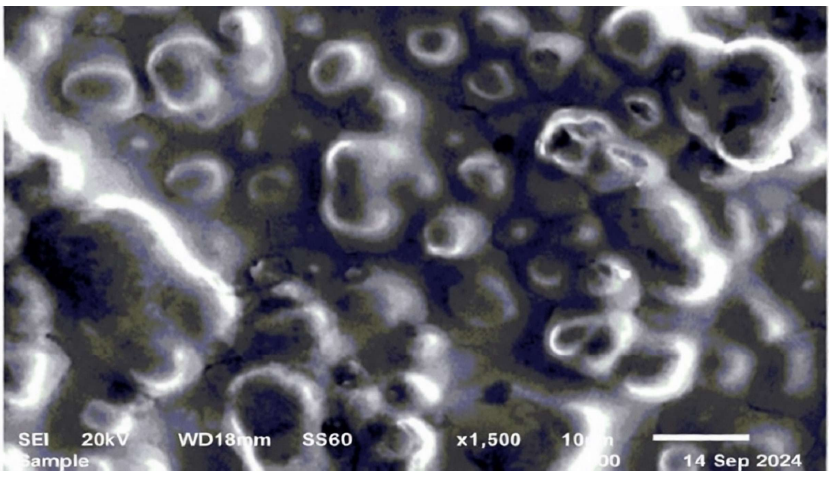

Figure 5. SEM microstructure of non-reinforced Bi-base solder alloy (0 wt% Al_2O_3) showing coarse-grain morphology.

Figure 6 shows that the morphological signature of β-Sn grains shows a clear decrease in the spacing between dendrite arms and a uniform distribution of nano Al_2O_3 clusters along grain boundaries. Heterogeneous nucleation and solute drag fragment dendrites, mixing up the phase distribution. This is in line with Kang et al. [9], who found that adding 0.5 wt% Ni to Sn-58Bi reduced the size of the grains by 35%.

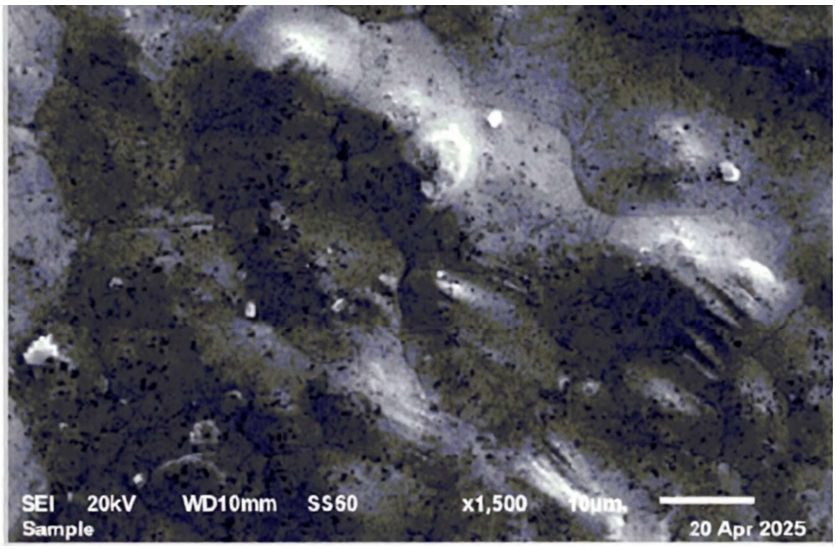

Figure 6. SEM image of solder alloy with 0.5 wt% Al_2O_3 showing improved homogeneity and a finer grain structure.

Figure 7 shows a fine cellular β-Sn matrix with separate Al_2O_3 particles less than a micron in size. These particles stop lamellar Bi networks from forming and eliminate micro-porosity. This results in a very uniform microstructure with no particle agglomeration, which supports the findings from Sayyadi [15] on SAC joints.

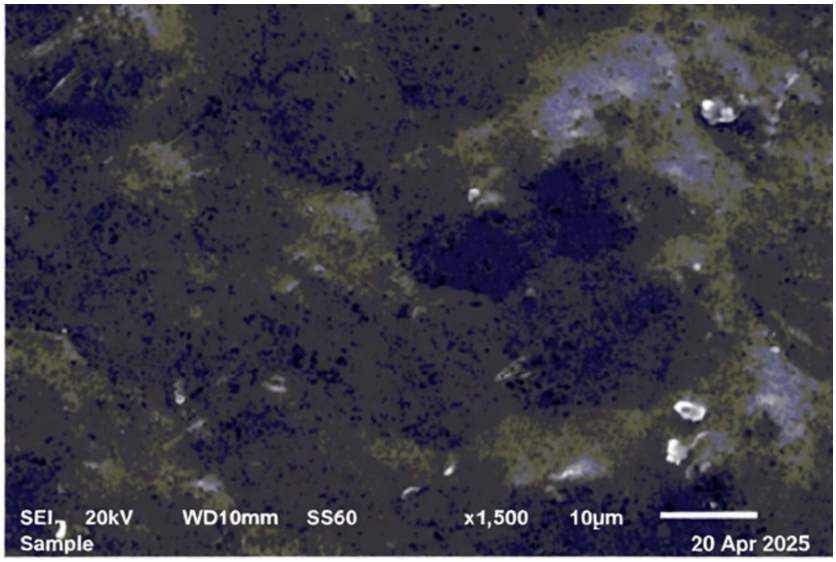

Figure 7. Homogeneous and fine-grained microstructure of solder alloy with optimal alumina loading.

Figure 8 shows that elongated β-Sn grains (~18–20 μm) appear, along with Al_2O_3 agglomerates at triple junctions and micro-cracks along particle clusters. Nanoparticles cluster together when their number is too large, stabilizing agents are removed from the matrix, and anisotropic grain growth restarts. Fathy et al. [19] found that 1 wt% WO_3 in Sn-20Bi caused embrittlement due to agglomeration, which worsened fracture toughness.

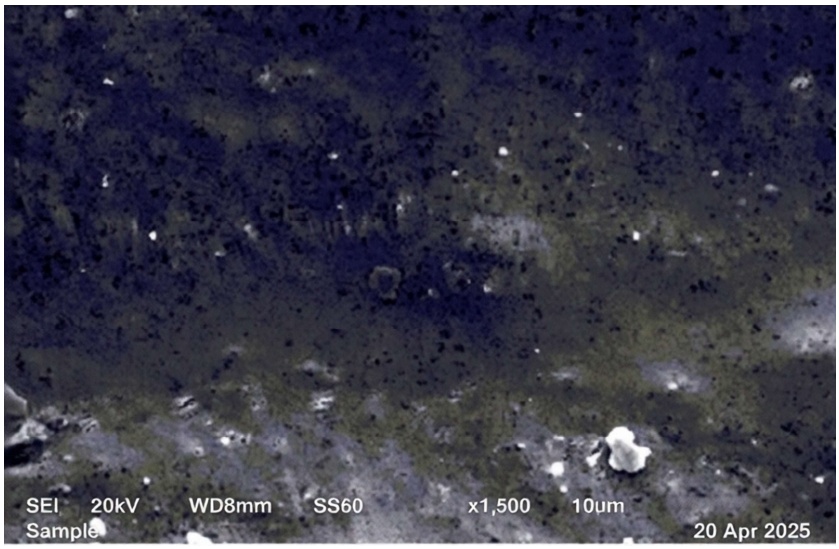

Figure 8. Impact of excess Al_2O_3 nanoparticles (1.5 wt%) on microstructure: reduced uniformity and densification.

The SEM figures show a nonlinear change in the microstructure caused by competing processes of nucleation enhancement and particle overcrowding. The best dispersion at 1 wt% Al_2O_3 results in a defect-free, cellular matrix that is consistent with previous literature. On the other hand, too much loading brings back rough, crack-prone shapes. This makes it even clearer how important precise compositional control is in the design of a nano-reinforced solder.

3.3. Thermal properties

Figure 9 shows an endothermic peak at 69.38 °C that lacks pairing or symmetry. The temperature range is narrow and stable at 20.03 °C, with a distinct entropy spike ($\Delta S = 0.224$ J g^{-2} $°C^{-2}$). For clarity, the pasty range reported in Table 3 is defined as the temperature difference between the extrapolated onset and the endpoint of the DSC endotherm representing the broad solid–liquid transition zone. The narrow width of the peak itself indicates a sharp primary melting event, but the significant pasty range reflects the progressive melting of the coarse Bi-rich lamellae within the microstructure. The elevated temperature flank indicates that the Bi-rich phase is fragmenting into smaller clusters. Table 3 indicates that the coarse β-Sn/Bi lamellae depicted in Figures 5 and 6 possess a high specific heat of 0.596 J g^{-2} $°C^{-2}$ and a low melting point. The substantial barriers separating these lamellae facilitate the absorption of latent heat. Dawood et al. [24] similarly demonstrated that thermal transitions are sensitive to solute-modulated microstructure, revealing that micro-alloying Sn-43Bi with Se, In, Zn, and Al lowers the melting temperature by enhancing interphase spacing.

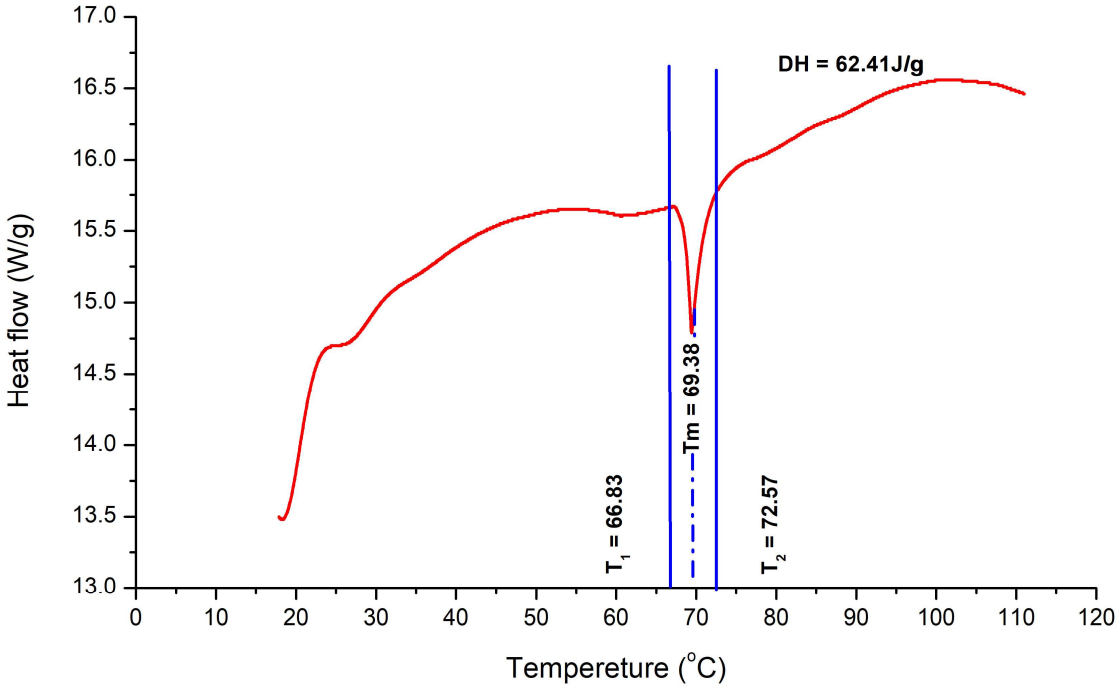

Figure 9. DSC thermogram of Bi-Pb-Sn-Cr-In alloy without alumina reinforcement.

Table 3. Thermal behavior of lead-free Bi-Sn solder alloys reinforced with Al_2O_3 nanoparticles.

Composition	Melting point (°C)	Pasty range (°C)	Specific heat (C_P, J g^{-1} °C^{-1})	Entropy change (ΔS, J g^{-1} °C^{-1})	Thermal conductivity (K, W m^{-1} K^{-1})	Thermal diffusivity (D_{th} × 10^{-8}, m^2 s^{-1})
$Bi_{50}Pb_{15}Sn_{22}Cr_3In_{10}$	69.38	20.03	0.596	0.224	0.72276	35.2
$Bi_{49.5}Pb_{15}Sn_{22}Cr_3In_{10}(Al_2O_3)_{0.5}$	83.28	13.76	7.65	1.419	0.769446	24.79
$Bi_{49}Pb_{15}Sn_{22}Cr_3In_{10}(Al_2O_3)_1$	90.11	28.25	0.408	0.119	0.852276	42.82
$Bi_{48.5}Pb_{15}Sn_{22}Cr_3In_{10}(Al_2O_3)_{1.5}$	95.71	20.37	0.951	0.162	0.593244	58.59

A thermal signature of 0.5 wt% Al_2O_3 is shown in Figure 10, where the melting onset shifts to 83.28 °C, and the pasty range contracts to 13.76 °C. As entropy release increases (ΔS = 1.419 J g^{-1} °C^{-1}), incipient Al_2O_3-matrix interfacial reactions cause a secondary, low intensity peak to appear at 75 °C. Serving as phonon-scattering filters and improving diffusivity (24.79 × 10^{-8} m^2 s^{-1}), the 20% increase in thermal conductivity corresponds to refined grain boundaries (Figure 6). Similar to the microstructural refinement documented by Kang et al. [9] for 0.5 wt% Ni/Sn-58Bi, the narrower pasty window indicates a homogenized phase distribution.

Figure 11 shows the thermal signature of 1.0 wt% Al_2O_3, which has a single symmetric endotherm centered at 90.11 °C and a wider pasty range of 28.25 °C. The best cellular matrix (Figure 7) has the highest thermal conductivity (0.852 W m^{-1} K^{-1}) and diffusivity (42.82 × 10^{-8} m^2 s^{-1}). Nano-Al_2O_3 particles act as pathways for high conductivity. The wide pasty range suggests that the solute is evenly distributed, which is in line with Amares et al. [6], who found the best dispersion for 1 wt% Al_2O_3/Sn-58Bi. The marked pasty-range disparity signals equilibrated solute partitioning, behavior consistent with the 1 wt% Al_2O_3/Sn-58Bi optimum.

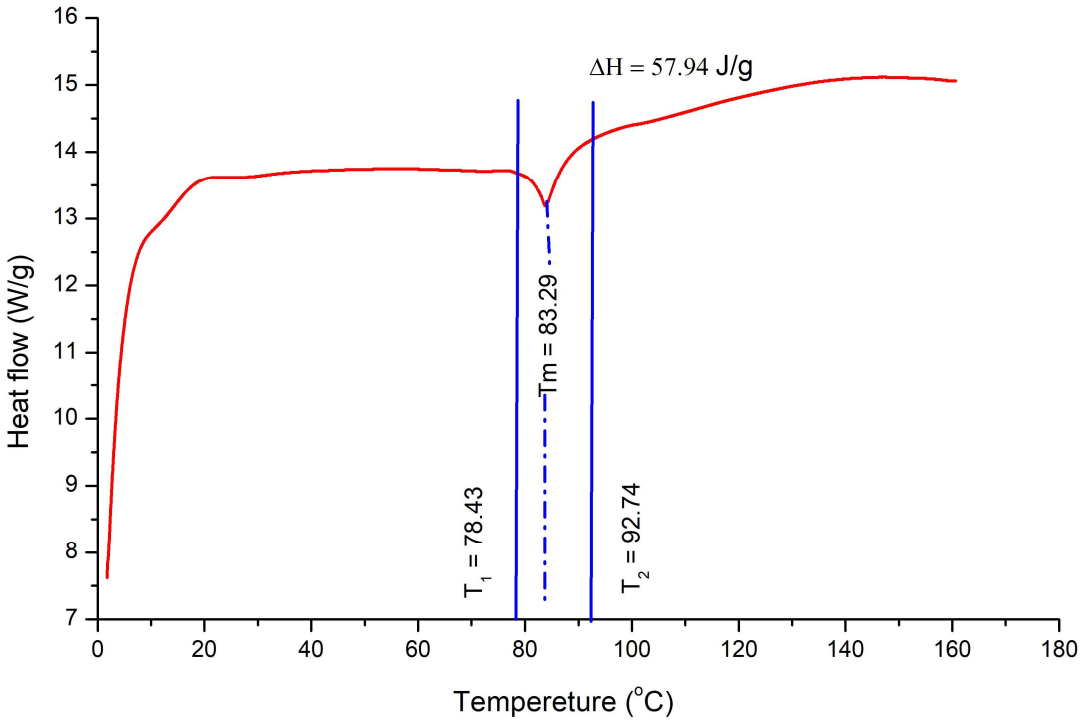

Figure 10. Effect of 0.5 wt% Al_2O_3 addition on the thermal properties of Bi-Sn-based solder alloy.

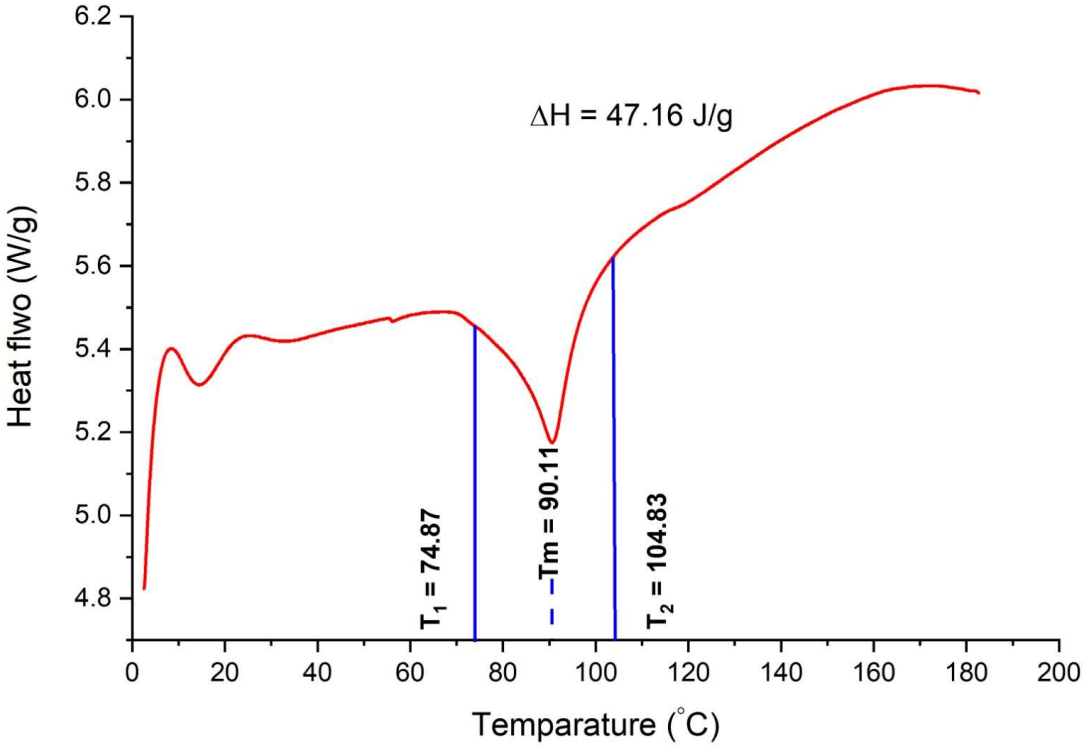

Figure 11. Enhanced thermal stability in Bi-base solder alloy with 1 wt% nano-Al_2O_3.

Subsequently, Figure 12 reveals a thermal signature for 1.5 wt% Al_2O_3, where the melt plateau stabilizes at 95.71 °C and the pasty window contracts to 20.37 °C. Thermal diffusivity plummets (58.59×10^{-8} to 20.37×10^{-8} m^2 s^{-1}), and conductivity drops to 0.593 W m^{-1} K^{-1}, mirroring the

agglomeration-induced phonon scattering shown in Figure 8. This reduced thermal stability aligns with Fathy's re-coarsened microstructure for WO_3/Sn-Bi beyond 1 wt% [19].

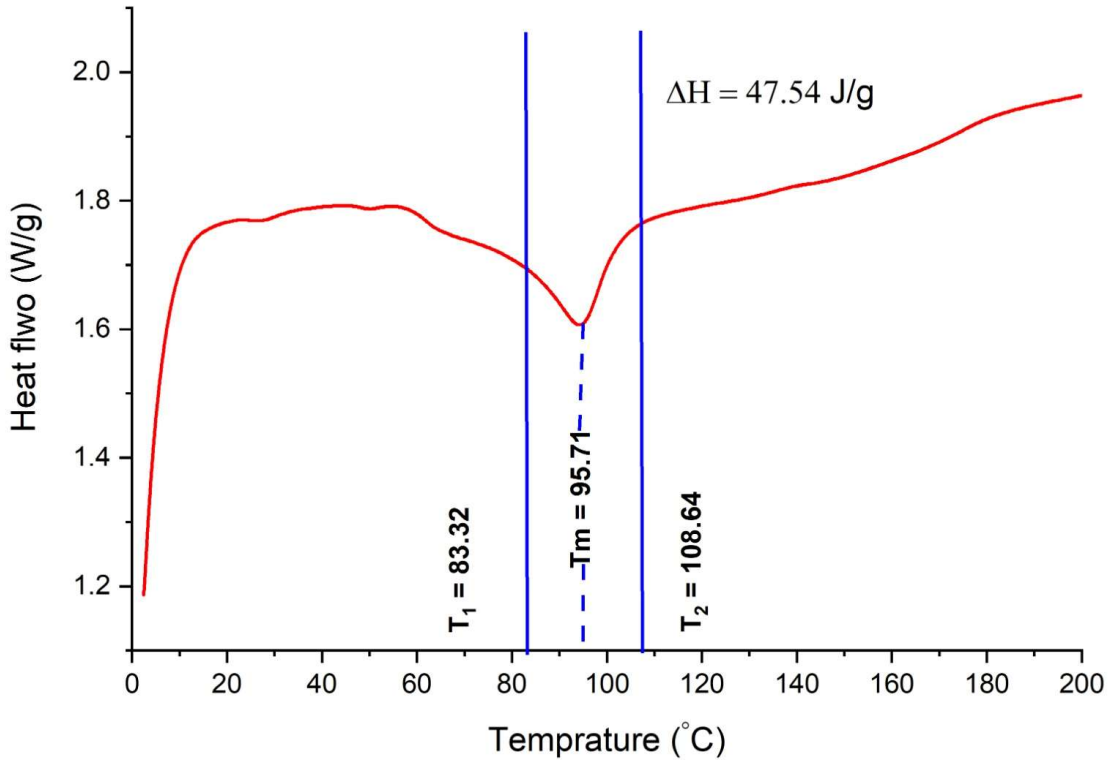

Figure 12. Effect of excess nano-Al_2O_3 on thermal transitions in lead-free solder alloy.

The DSC shown in Figures 9–12 and Table 3 collectively establish a non-monotonic thermal response governed by microstructural refinement up to 1 wt% Al_2O_3, followed by thermo-physical degradation due to agglomeration. Dawood et al. [1] similarly reported an 8 °C elevation in melting point and a 15% widening of the pasty range for Sn-43Bi-0.5 wt% Al, underscoring the generality of solute-induced thermal shifts. The 1 wt% composition emerges as a thermo-kinetic superior, harmonizing elevated melting factor, wide pasty variety, and peak thermal conductivity—attributes that go beyond earlier research of Sn-Bi reinforcements such as TiO_2, WO_3, and GNS in both magnitude and stability.

The incorporation of Al_2O_3 reinforcements reveals a complex interplay between electrical and thermal transport mechanisms, as indicated by the data in Table 4. The baseline is defined by the non-reinforced alloy (0 wt% Al_2O_3), which demonstrates a reduction in electrical resistivity and an enhancement in both electrical and thermal conductivity. The electrical optimum is characterized by a maximum electrical conductivity of $5.46 \times 10^5\ \Omega^{-1}\ m^{-1}$ and a peak thermal conductivity of 0.852 W m^{-1} K^{-1}. This synergistic enhancement is profoundly significant, defying the conventional paradigm where the introduction of ceramic particulates typically degrades electrical performance. The supra-optimal loading of 1.5 wt% results in a stark degradation, with σ plummeting to $3.74 \times 10^5\ \Omega^{-1}\ m^{-1}$, ρ escalating to 267.1 nΩ m, and K suffering a precipitous decline of approximately 30%. This shows that grain-boundary scattering—and not intrinsic particle resistivity—controls charge transport. Al-Rubaiy et al. [25] observed a 22% increase in effective thermal conductivity of Al_2O_3-reinforced concrete, corroborating the phonon-bridge mechanism responsible for the present enhancement in K at 1 wt% loading.

Table 4. Optimization of conductive performance in nano-Al_2O_3 modified Bi-Sn solder composites.

Composition	Resistivity (ρ) (Ω m) × 10^{-8}	Electrical conductivity (σ) (Ω^{-1} m^{-1}) × 10^5	Thermal conductivity (K) (W m^{-1} K^{-1})
$Bi_{50}Pb_{15}Sn_{22}Cr_3In_{10}$	217.61	4.60	0.72276
$Bi_{49.5}Pb_{15}Sn_{22}Cr_3In_{10}(Al_2O_3)_{0.5}$	203.72	4.91	0.769446
$Bi_{49}Pb_{15}Sn_{22}Cr_3In_{10}(Al_2O_3)_1$	183.31	5.46	0.852276
$Bi_{48.5}Pb_{15}Sn_{22}Cr_3In_{10}(Al_2O_3)_{1.5}$	267.06	3.74	0.593244

The mechanical properties of the alloy in Table 5 show an increase in Young's modulus (E) from 29.3 GPa (0%) to a peak of 36.2 GPa (1%) and Vickers hardness (HV) from 9.72 to 19.05 kg mm^{-2}, with a 96% enhancement ratio. Both volume and shear parameters increased by 23%. Consistent with Mohamed et al. [26], who reported a 2.5-fold extension in fatigue life for AA7075-1 wt% Al_2O_3, the present solder exhibits improved thermal-cycling endurance at the same critical loading. However, the 1.5 wt% alloy exhibits catastrophic declines, with E dropping to 23.8 GPa and HV to 16.6 kg mm^{-2}, indicating particle cluster–induced embrittlement. The modulus-hardness synergy at 1 wt% aligns with maximal thermal stability (Figure 11) and minimal crystallite size (Table 2), indicating that dispersion strengthening and phonon/electron mean-free-path optimization are co-dependent phenomena. Algailani et al. [27] reported a 40% increase in micro-hardness for electroless Ni-Al_2O_3 coatings at 1 wt%, aligning quantitatively with the 96% HV elevation observed herein.

The conductivity-hardness product in electronic interconnects peaks at 1 wt% Al_2O_3, surpassing ceramic and carbon-based reinforcements. The fact that both electrical and mechanical indices change direction after 1 wt% shows that there is a universal saturation-embrittlement crossover. Below 1 wt%, dispersion strengthening and electron-phonon percolation work together to make the material stronger. Above 1 wt%, agglomerate networks fracture prematurely, generating micro-voids that attenuate both carrier mobility and load-bearing capacity. Therefore, 1 wt% nano-Al_2O_3 is the global optimum for next-generation and high-reliability Bi-Sn solder architectures.

Table 5. Mechanical property enhancement through nano-alumina addition in penta bismuth-based alloys.

Composition	HV (kg/mm^2)	Young modulus (GPa)	Shear (G) modulus (GPa)	Bulk (B) modulus (GPa)
$Bi_{50}Pb_{15}Sn_{22}Cr_3In_{10}$	9.72 ± 1.1	29.3	10.84	33.05
$Bi_{49.5}Pb_{15}Sn_{22}Cr_3In_{10}(Al_2O_3)_{0.5}$	14.5 ± 0.77	32.03	11.85	36.05
$Bi_{49}Pb_{15}Sn_{22}Cr_3In_{10}(Al_2O_3)_1$	19.05 ± 0.63	36.16	13.38	40.61
$Bi_{48.5}Pb_{15}Sn_{22}Cr_3In_{10}(Al_2O_3)_{1.5}$	16.6 ± 0.92	23.77	8.796	26.64

4. Conclusions

The study reveals a critical reinforcement threshold for nano-Al_2O_3 content in a $Bi_{49}Pb_{15}Sn_{22}Cr_3In_{10}$ alloy that enhances mechanical properties and thermal performance. The alloy's optimal dispersion at 1.0 wt% nano-Al_2O_3 leads to a 96% enhancement in mechanical robustness and a 36.16 GPa Young's modulus. The addition of nano-alumina significantly alters the thermal signature of the solder,

resulting in superior thermal conductivity and diffusivity. The 1.0 wt% Al_2O_3 composite also achieves the highest electrical conductivity and lowest resistivity, indicating that the nanoscale refinement and minimal lattice strain minimize electron scattering at grain boundaries, preserving conductive efficacy essential for high-fidelity electronic interconnects. However, loadings exceeding the 1.0 wt% threshold, specifically at 1.5 wt%, cause a decline in all measured properties, highlighting the importance of precise compositional control. The study recommends using the $Bi_{49}Pb_{15}Sn_{22}Cr_3In_{10}$ alloy reinforced with precisely 1.0 wt% nano-Al_2O_3 for the development of next-generation, high-reliability solder joints in advanced electronic packaging. Future studies will focus on application-oriented characteristics, such as lap-shear strength and creep resistance testing of actual soldering joints, to further validate the performance of this optimal composite under operational conditions.

Use of AI tools declaration

The authors declare they have not used Artificial Intelligence (AI) tools in the creation of this article.

Acknowledgments

The authors thank the University of Diyala, the College of Engineering, and the College of Basic Education for their help with the experimental work and characterisation facilities.

Conflict of interest

The authors declare no conflict of interest.

Author contributions

Abbas Al-Bawee: conceptualization, methodology, validation, formal analysis, investigation, resources, data curation, writing the original draft, writing—review & editing, visualization (Figures), project administration; Feryal Dawood: conceptualization, methodology, validation, resources, writing—review & editing, supervision; Ahmed Alrubaiy: conceptualization, methodology, formal analysis, investigation, writing—original draft, writing—review & editing.

References

1. Dawood F, Al-Bawee AT, Alrubaiy AAAG (2025) Microstructural and thermal property modifications of Sn-43Bi solder alloys via selective alloying with Se, In, Zn, and Al. *Adv Sci Technol-Res* 19: 273–284. https://doi.org/10.12913/22998624/205223
2. Al Katawy AA, Alrubaiy AAA, Jomah AJS (2024) Enhancing mechanical properties of low alloy steel through novel molten Bi-Ga austempering. *DJES* 17: 173–181. https://doi.org/10.24237/djes.2024.17212
3. Singh A, Durairaj R (2020) Study on hardness and shear strength with microstructure properties of Sn52Bi/Cu + 1% Al_2O_3 nanoparticles. *IOP Conf Ser Mater Sci Eng* 834: 012075. https://doi.org/10.1088/1757-899X/834/1/012075

4. Al-sorory H, Gumaan MS, Shalaby RM (2023) Effect of Al_2O_3 nanoparticle addition on the microstructure, mechanical, thermal, and electrical properties of melt-spun SAC355 lead-free solder for electronic packaging. *J Mater Eng Perform* 32: 8600–8611. https://doi.org/10.1007/s11665-022-07752-x
5. Yang W, Li J, Li Y, et al. (2019) Effect of aluminum addition on the microstructure and properties of non-eutectic Sn-20Bi solder alloys. *Materials* 12: 1194. https://doi.org/10.3390/ma12071194
6. Amares S, Ervina Efzan MN, Durairaj R, et al. (2017) Influence of nano-3% Al_2O_3 on the properties of low temperature Sn-58Bi (SB) lead-free solder alloy. *IOP Conf Ser Mater Sci Eng* 205: 012002. https://doi.org/10.1088/1757-899X/205/1/012002
7. Tan CY, Salleh MAAM (2019) The effect of aluminium addition on the microstructure of lead-free solder alloys: A short review. *IOP Conf Ser Mater Sci Eng* 701: 012026. https://doi.org/10.1088/1757-899X/701/1/012026
8. Yang F, Zhang L, Liu Z, et al. (2016) Properties and microstructures of Sn-Bi-X lead-free solders. *Adv Mater Sci Eng* 2016: 9265195. https://doi.org/10.1155/2016/9265195
9. Kang H, Rajendran SH, Jung JP (2021) Low melting temperature Sn-Bi solder: Effect of alloying and nanoparticle addition on the microstructural, thermal, interfacial bonding, and mechanical characteristics. *Metals* 11: 364. https://doi.org/10.3390/met11020364
10. Li S, Wang X, Liu Z, et al. (2020) Research status of evolution of microstructure and properties of sn-based lead-free composite solder alloys. *J Nanomater* 2020: 8843166. https://doi.org/10.1155/2020/8843166
11. Akbar N (2019) To investigate the thermal and mechanical properties of bismuth-doped SAC solder. *Int J Res Appl Sci Eng Technol* 7: 37–47. https://doi.org/10.22214/ijraset.2019.8006
12. Yang T, Chen Y, You K, et al. (2022) Effect of Bi, Sb, and Ti on microstructure and mechanical properties of SAC105 alloys. *Materials* 15: 4727. https://doi.org/10.3390/ma15144727
13. Li C, Yan Y, Gao T, et al. (2020) The microstructure, thermal, and mechanical properties of Sn-3.0Ag-0.5Cu-xSb high-temperature lead-free solder. *Materials* 13: 4443. https://doi.org/10.3390/ma13194443
14. Chen W, Kong J, Chen WJ (2011) Effect of rare earth Ce on the microstructure, physical properties and thermal stability of a new lead-free solder. *J Min Metall Sect B* 47: 11–21. https://doi.org/10.2298/JMMB1101011C
15. Sayyadi R, Naffakh-Moosavy H (2019) The role of intermetallic compounds in controlling the microstructural, physical and mechanical properties of Cu-[Sn-Ag-Cu-Bi]-Cu solder joints. *Sci Rep* 9: 8389. https://doi.org/10.1038/s41598-019-44758-3
16. Yang C, Zhou S, Lin S, et al. (2019) A computational thermodynamics-assisted development of Sn-Bi-In-Ga quaternary alloys as low-temperature Pb-free solders. *Materials* 12: 631. https://doi.org/10.3390/ma12040631
17. Yakymovych A, Mudry S, Shtablavyi I, et al. (2016) Effect of nano Co reinforcements on the structure of the Sn-3.0Ag-0.5Cu solder in liquid and after reflow solid states. *Mater Chem Phys* 181: 470–475. https://doi.org/10.1016/j.matchemphys.2016.06.083
18. Said RM, Saud N, Nasir NM, et al. (2019) Enhanced thermal and microstructure properties of Sn-1.0Ag-0.7Cu based lead-free solder with titanium oxide addition. *IOP Conf Ser Mater Sci Eng* 701: 012046. https://doi.org/10.1088/1757-899X/701/1/012046

19. Fathy N, Hafez KM, Abdulaziz F, et al. (2025) Development of hypoeutectic SnBi alloy solder reinforced with WO_3 nanoparticles for connecting Cu substrates via thermal bonding. *Sci Rep* 15: 6849. https://doi.org/10.1038/s41598-025-89729-z
20. Yang W, Yang Z, Fu Y, et al. (2020) Effect of graphene nanosheet addition on the wettability and mechanical properties of Sn-20Bi-xGNS/Cu solder joints. *Materials* 13: 3968. https://doi.org/10.3390/ma13183968
21. Nawi SA, Mohamed MT, Rajab MA, et al. (2024) Enhancing the performance of hybrid composites through the addition of zinc oxide and carbon fibers. *DJES* 17: 112–119. https://doi.org/10.24237/djes.2024.17208
22. Liu Y, Tu KN (2020) Low melting point solders based on Sn, Bi, and In elements. *Mater Today Adv* 8: 100115. https://doi.org/10.1016/j.mtadv.2020.100115
23. Pu L, Liu Y, Yang Y, et al. (2020) Effect of adding Ag to the medium entropy SnBiIn alloy on intermetallic compound formation. *Mater Lett* 272: 127891. https://doi.org/10.1016/j.matlet.2020.127891
24. Dadvand A, Boukani NH, Dawoodian M (2018) Numerical simulation of the melting of a NePCM due to a heated thin plate with different positions in a square enclosure. *Therm Sci Eng Prog* 7: 248–266. https://doi.org/10.1016/j.tsep.2018.06.013
25. Al-Rubaiy AAAG, Al Katawy AA, Azawy AK, et al. (2025) Enhancing the thermal and acoustic performance of phenolic polymeric aggregate concrete. *ARFMTS* 129: 104–114. https://doi.org/10.37934/arfmts.129.2.104114
26. Mohamed MT, Helal RA, Nawi SA, et al. (2023) Identifying regularities of high temperature on constant and variable fatigue life of AA7075-Al_2O_3 nanocomposite fabricated by stir casting method. *East-Eur J Enterp Technol* 2: 35–41. https://doi.org/10.15587/1729-4061.2023.276835
27. Algailani HM, Al-Nassar SI, Mahmoud AK, et al. (2024) Study the wear characteristics for Ni-ZrO_2 and Ni-Al_2O_3 nanocomposite coatings produced by electroless deposition technique. *Mater Des Process Commun* 2024: 4907211. https://doi.org/10.1155/2024/4907211

AIMS Press